Proceedings of ASME Turbo Expo 2011
GT2011
June 6-10, 2011, Vancouver, British Columbia, Canada

GT2011-46677

QUANTIFYING OPTICAL TIP-TIMING PROBE ERROR WITH LABORATORY APPARATUS

Bruce D Hockaday
Pratt & Whitney
East Hartford, Connecticut 06108, USA

Abstract

Detection of airfoil time of arrival with optical probes has been evolving since the 1980s. Time of arrival data are used to infer airfoil stresses caused by vibration through a sequence of manipulations. The data conversion begins by converting arrival time to blade position, so blade deflection can be determined from the expected non-vibrating position. Various methods are used in the industry to convert deflection data to frequency, amplitude, and stress, which is beyond the scope of this paper. Regardless of the analytical approach used, producing accurate stress information relies on the precise detection and measurement of time of arrival, which equates to blade position.

Recent improvements have been made in time of arrival system accuracy by running faster clocks to increase temporal resolution of the measurement. Greater timing resolution, afforded by clock speed, will have diminishing returns when probe and blade-tip interactions begin producing dominant errors. In the case of optical probes, the blade-tip needs to be treated as a curved reflector in the optical system that is capable of introducing dynamic errors. In engine operation the blade-tip moves axially under the probe from untwist, static deflection, and vibration, causing the light to reflect from different parts of the blade-tip. This relative movement between the probe and blade-tip cause the arrival time to change dynamically. Neglecting the dynamic arrival errors caused by the blade-tip's optical properties will result in blade deflection-errors that propagate into the stress information.

This paper presents a laboratory study that quantifies time of arrival errors due to optical interaction with tip radii. The study reports measured arrival position error as a function of location and optical signal power levels. The work is presented in terms of arrival position, producing information that is independent of rotational speed, and vibratory mode.

Introduction

A common misconception with tip-timing measurements is that optical probes detect the blade-tip when first hitting the probe's light beam. When recognized that this is not true, the next misconception is that all delay errors are constant between blade-tip incursion into the light beam and recording blade arrival time. If this last assumption were true, the constant timing error would drop out when calculating the vibration induced deflection. This assumption may not hold up when the vibration produces an axial displacement of the blade relative to the probe beam. Understanding this potential error becomes important when the blade-tip edge radius varies at the point of probe beam intersection with the blade.

The front-end of optical tip-timing systems will record the blade's time of arrival based on the analog signal generated by each blade passing a probe. Each blade passage signal can be monitored with an electronic threshold circuit that initiates recording the time of arrival. This time record is derived from satisfying the threshold setting and recording the counter based on front-end system's fixed frequency computer clock. The clock frequency defines the temporal resolution of this type of tip-timing system. These time records are converted to blade-tip arrival locations by knowing the engine speed and blade tip's circumferential path length information.

Deriving vibratory stress information starts by calculating a vibration-induced blade-tip deflection for use in stress analysis algorithms. The deflection is calculated by subtracting a non-vibrating arrival location from a vibrating arrival location.

This subtraction removes errors common to both arrival locations. When the errors are equal there is no need to know the true blade arrival location. However, this assumption will not hold up when delay errors change with vibration. Some modes of vibration produce enough axial blade movement to cause the probe to intersect a different part of the blade-tip edge radius. The new edge radius will result in a changing blade-tip incursion into the probe beam, thus changing the delay error. This study will show how much delay error occurs with an unfocussed optical spot probe for a given change in blade-tip radius. Future work will compare these results with a focused optical spot probe.

Laboratory Apparatus

This laboratory study evaluates arrival location error with a test specimen having one edge with a varying radius of curvature. The laboratory environment helps eliminated other error sources providing unambiguous results with a simple test apparatus.

The experiment required measuring the optical power collected by the probe from light that backscattered from an object with a radius and recording the object location. This requirement was met by recording the probe's output signal with respect to the relative position of a specimen with known edge radius. The apparatus used to do this included an unfocused spot probe, a computer controlled micro positioning system, an optical power meter and a test specimen with known geometry.

The testing apparatus was assembled primarily from commercially available optical table fixtures, Fig. 1. The probe mounting equipment was comprised of a pair of 2 inches (50.8mm) diameter posts mounted to the optical table top to support the probe and reduce vibration. Two platform brackets are attached to the 2 inches (50.8 mm) posts, providing a means for attaching the probe mounting plate as well as allowing course vertical adjustment. The custom probe mounting plate had a groove and set screw arrangement to clamp and align the unfocused optical spot probe.

The unfocused spot probe was composed of seven optical fibers housed in 0.0625 inches (1.588mm) outside diameter hypo tube. The fibers were arranged with a center transmission fiber and six receiver fibers were arranged in a circle around the center fiber. All fibers were 100 micron core with 0.22 numerical aperture (NA).

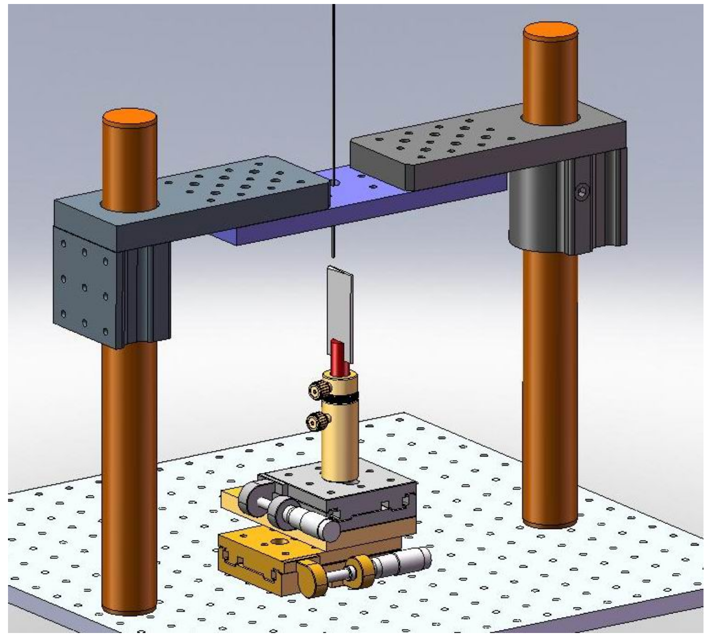

FIG. 1, LABORATORY APPARATUS WITH UNFOCUSED SPOT PROBE ABOVE TEST SPECIMEN

The specimen scanning system was comprised of two translation stages and a top mounted 0.5 inches (12.7mm) diameter post holder to mount the test specimen. The translation stages were joined orthogonally and attached to the table. This provided 2 square-inches (50.8square-mm) scanning area. The 0.5 inches (12.7mm) post holder had an elevating screw allowing manual adjustment of the gap between the probe tip and the top surface of the specimen. The elevating screw thread provided 0.0313 inches (0.794mm) lift per turn. The test specimen was attached to a 0.5 inches (12.7mm) diameter post with a clamp arrangement. Although not shown, the translation stages were equipped with stepper motors to allow computer control of the movement within the scanning plain. Each stepper motor had a 2 inches (50.8mm) range and required 256 steps per 0.001 inches (0.0254mm) movement.

Figure 2 shows a model of the test specimen that was fabricated from 0.090 inches (2.286mm) thick titanium sheet stock. The stock was cut into a rectangle approximately 1.25 by 3 inches (31.75 by 76.2mm) and mounted vertically so that the 1.25 by 0.090 inches (31.75 by 2.286mm) surface represents the airfoil tip. Scanning the probe beam across the 0.090 inches (2.286mm) direction represents rotation or circumferential movement of a blade under a probe. Scanning along the 1.25 inches (31.75mm) direction represents axial movement of a blade.

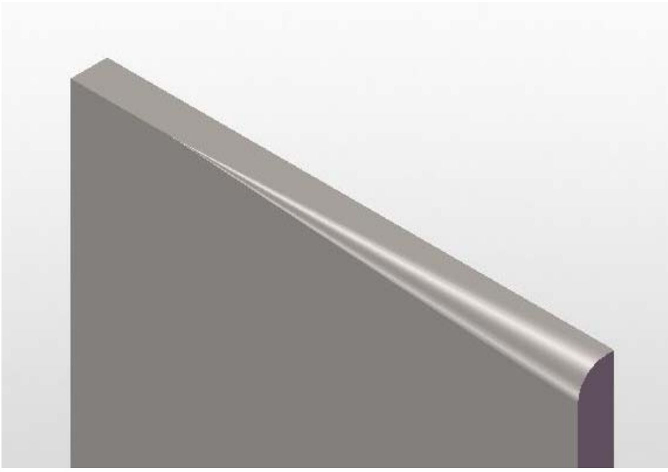

FIG. 2; TEST SPECIMEN SHOWING VARYING EDGE RADIUS

The top surface of the specimen was flattened with an end mill and lapped with 320 grit wet/dry abrasive paper. One edge of the top surface was altered, producing a varying radius that ranged from 0.0 to 0.0625 inches (0.0 to 1.5875mm). This was done by hand with periodic inspection using a set of machinist's radius gages, sizes 0.03125, 0.0469 and 0.0625 inches (0.79375, 1.19126 and 1.5875mm). The final edge radii were finished with 320 wet/dry paper to blend any discontinuities and match the surface finish of the top surface.

The automated test system includes, the computer, optical power meter, and stepper motors. The computer only read the power meter measurements, all meter settings are entered manually. The computer sends each motor step commands to move the translation stages. The translation stage location information was inferred by counting motor steps.

The computer's operator interface is used to define the scanning parameters and run the test. At startup, the stepper motor system is run through a homing operation, typical of computer controlled positioning systems. This established an absolute zero location when each motor is fully retracted. The operator enters a local origin in absolute coordinates to define the starting point of a scan. A scan range is also entered to limit the scan size and prevent traveling beyond the equipment's range. In practice, the operator moved the specimen with the motors and observed the power meter to determine the local origin and scan ranges. The resulting data files recorded optical power as a function of relative position within the scanning area. The last entry the operator makes is the number of absolute steps to travel between each measurement. This defines the spatial resolution of the measurement. The spatial resolution for axial and circumferential directions were set independently allowing greater data detail in one direction as compared to the other.

Data collection

The unfocused spot probe was mounted in the bench top apparatus and the gap to the specimen set. The probe was powered with a multimode near infrared laser operating at 830nm wavelength. The laser driver was set to an output power of 43mW that was measured at the probe tip. The optical power was held constant throughout the entire experiment. The measurement step was set to 0.050 inches (1.27mm) along the length of the specimen, the axial direction. The orthogonal measurement step, the circumferential direction, was set to 0.005 inches (0.127mm) since higher spatial resolution was needed to see the effect of the edge radii. Data were collected at three different probe-to-specimen gaps, 0.0625, 0.188 and 0.25 inches (1.588, 4.763 and 6.35mm), Figs. 3, 4 and 5 respectively.

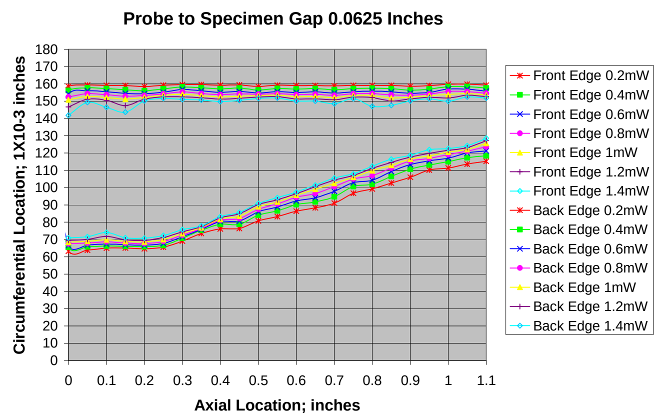

FIG. 3; EDGES DETECTED AT SPECIFIED OPTICAL POWER LEVELS WITH PROBE 0.0625 INCHES FROM SPECIMEN

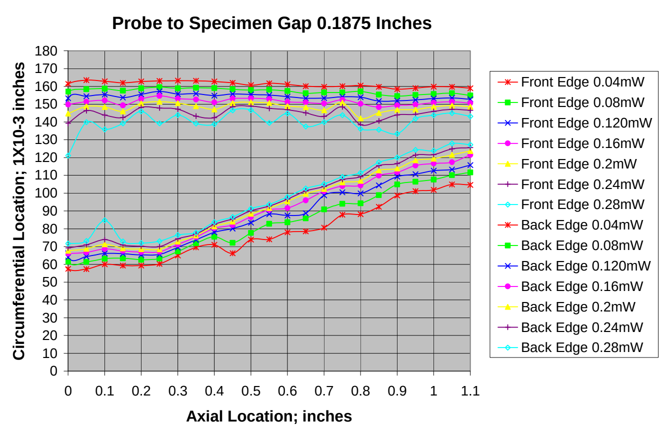

FIG. 4; EDGES DETECTED AT SPECIFIED OPTICAL POWER LEVELS WITH PROBE 0.1875 INCHES FROM SPECIMEN

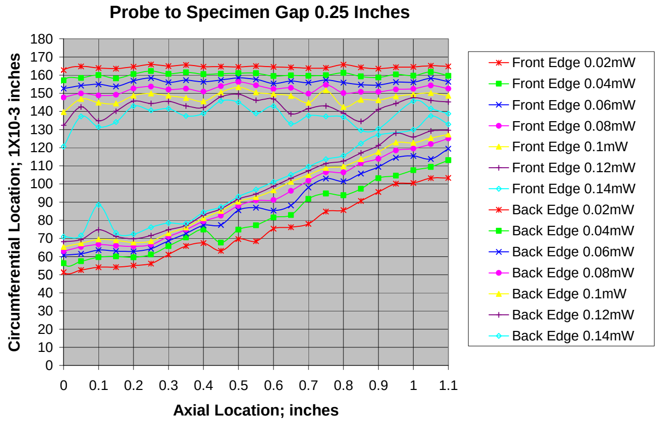

FIG. 5; EDGES DETECTED AT SPECIFIED OPTICAL POWER LEVELS WITH PROBE 0.25 INCHES FROM SPECIMEN

The data in Figs. 3 through 5 are plotted with the axial location along the specimen length as the independent variable. The axial location is also proportional to the specimen's edge radii. The dependent variable is the circumferential location of the specimen where the received optical power is at a specified level. Each optical power level simulates a threshold circuit trigger level in the front-end of the tip-timing measurement system. The spatial resolution in the circumferential direction was improved by linear interpolation of the data interval containing the set power level. Errors in finding the specimen edge are the difference between the true and detected edge locations in the circumferential direction.

Experimental Results

The data in each figure are grouped into two families of curves produced by detecting the front and back edges of the specimen. Each curve in the group is defined by a specific level of optical power collected and measured at the detector. These power levels are equivalent to the trigger level set in the tip timing front end system. There is only one trigger level that can identify the true edge location. All other trigger levels must contain an offset error causing early or late detection.

The data collected at the 0.0625 inches (1.588mm) probe gap, Fig. 3, shows trends typical of all plotted data but with less noise. The unaltered back edge of the specimen can be identified in the data as the group of straight lines that are at constant circumferential locations, between 0.150 and 0.160 inches on the graph. The front edge data has two sections with an inflection point at 0.2 inches in axial location. The front edge data that are parallel to the back edge represent the original specimen's sharp edge, located between 0.0 and 0.2 inches in the axial direction. The data from the specimen's original sharp front edge provide an unambiguous reference for quantifying errors caused by edge radii even though the true edge location is unknown.

The data from the original specimen's sharp edges show that perceived edge location within a data set changes with received optical power levels. Knowledge of the specimen thickness allows estimating the power level that identifies the true sharp edge locations. As an example the 0.6mW power level data collected at 0.0625 inches (1.588mm) probe gap identifies the true edge locations since the distance between the front and back signals is 0.090 inches (2.286mm), Fig. 6. The trigger levels matching the true edges for probe gaps of 0.188 inches (4.763mm) and 0.25 inches and (6.35mm) are 0.12mW and 0.06mW respectively.

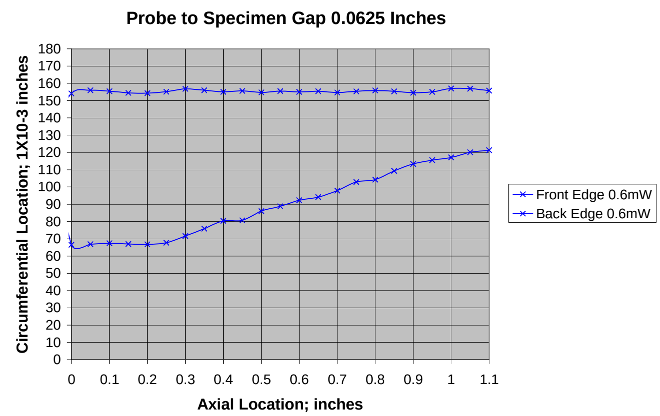

FIG. 6; TRUE EDGE DETECTED AT 0.6mW TRIGGER LEVEL WITH 0.0625 INCHES FROM SPECIMEN

The influence of edge radius on edge detection can be seen in the data beyond 0.2 inches, axial location. The edge radius causes the specimen's edge to be detected late compared to the sharp edge location. The delay in edge detection increases with increasing radius since the radius of curvature is largest at 1.1 inches axial location.

Discussion

The arrival errors observed in these experiments can be explained by applying geometric optic principles and simplifying assumption. Analysis hinges on applying the law of reflection to the probe beam interaction with the specimen. The law states that any incident ray will reflect from the surface at an angle that is equal, but opposite, of the incident ray when the angle is measured relative to the instantaneous surface normal. The lapped surface causes forward scattering of the reflected ray resulting in an angular spreading of the light about the reflected ray path. The forward scattering will be ignored as a simplifying assumption. Application of geometric ray tracing will simplify the analysis but will also ignore the intensity variation caused by the negative power of the curved edge and gap changes.

The optical properties of the unfocused probe are defined by the optical fiber. The fiber's numerical aperture (NA), 0.22, defines both the acceptance and transmission maximum cone angle, 12.7 degrees around the optic axis of the fiber. The probe's transmitted light beam has a Gaussian intensity profile where the intensity peak is on axis. The Gaussian nature of the transmitted beam profile will be simplified by approximating the beam width as the half intensity ray that occurs at 8 degrees off axis.

The probe interaction with the original sharp edge is looked at first, with the 0.0625 inches (1.588mm) probe specimen gap, Fig. 7. The probe is located with the first reflected light ray entering a receiver fiber, representing the lowest possible signal power level. This occurs when the probe center line is 0.005 inches (0.127mm) in front of the sharp edge. In this position the balance of the reflected light from the diverging beam will not intersect the probe, but rather goes to the right side of the probe, as illustrated in Fig 7. The remainder of the probe beam does not reflect and continues diverging in front of the specimen. This location has the lowest possible signal level, representing the largest early edge detection error for the sharp edge. By similarity, the probe center line will move 0.005 inches (0.127mm) past the sharp edge to fully illuminate all the receiver fiber with reflected light, reaching the highest collected power level. The analysis shows that the maximum range of sharp edge detection error is 0.010 inches (0.254mm).

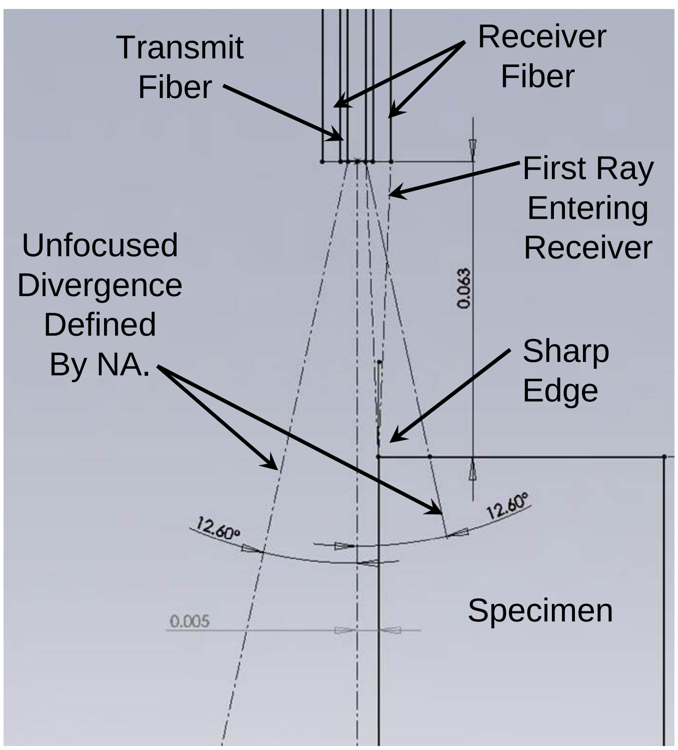

FIG. 7; RAY TRACING DIAGRAM OF ORIGINAL SHARP EDGE

The 0.010 inches (0.254mm) error range between lowest and highest signal power levels at the original sharp edges is in agreement with the data in Fig.3 where the probe gap is 0.0625 inches (1.588mm). This theoretical sharp edge detection error range applies to all probe gaps since is the geometry proves independent of the probe gap. The original sharp edge data in Figs. 4 & 5 shows a range of error that is 2 to 3 times larger than the ray tracing model predicts, suggesting that forward scattering is relevant at large gaps.

The probe interaction with the edge radius will be looked at for the full NA for the transmitted beam first. Figure 8 shows the ray tracing diagram for the 0.0625 inches (1.588mm) probe gap above the largest edge radius that is also 0.0625 inches (1.588mm). The three principle rays shown are the two define by the NA of the fiber and the center ray. The probe is located where the first possible ray enters a receiver fiber, putting the probe's center line 0.028 inches (0.711mm) past the true edge. This does not agree with the 0.052 inches (1.321mm) shown in the data, Fig. 3, suggesting that the Gaussian beam profile needs to be included in the analysis.

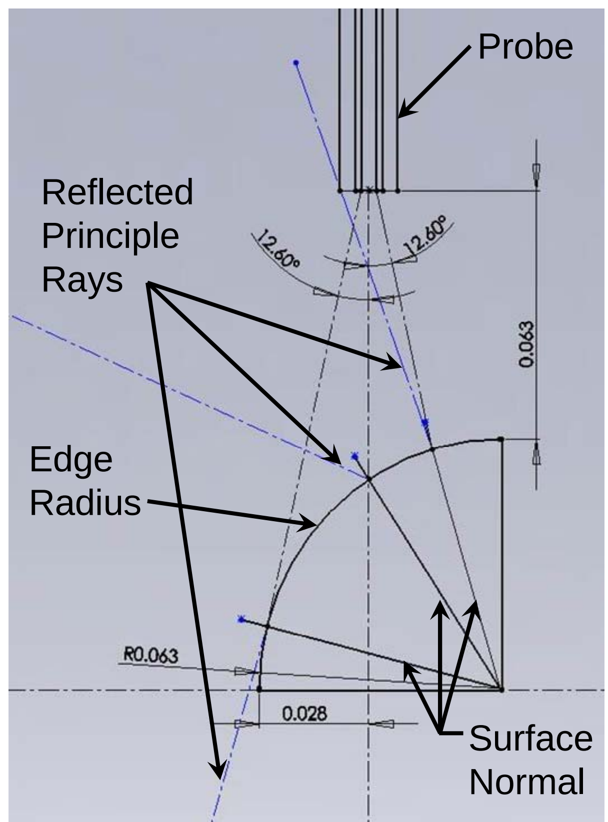

FIG. 8; RAY TRACING OF FIRST POSSIBLE DETECTED REFLECTION

The edge detection error associated with low signal power level is evaluated with the Gaussian assumption included, Fig. 9. This ray tracing diagram assumes first detection, or lowest measured power, of the radius edge occurs when the Gaussian beam perimeter first reflects back to center of the probe. Defining the lower power case this way permits a simple expression to describe the probe location as a function of edge radii. Under this assumption the incident and reflected Gaussian rays overlap and coincide with the surface normal. The resulting angle of the surface normal is equal to the angle defined by the half power point of the beam profile, 8 degrees. The resulting late edge detection of 0.045 inches (1.143mm) is closer to the 0.052 inches (1.321mm) in Fig. 3. Unlike the sharp edge case, the probe location is dependent on the probe gap.

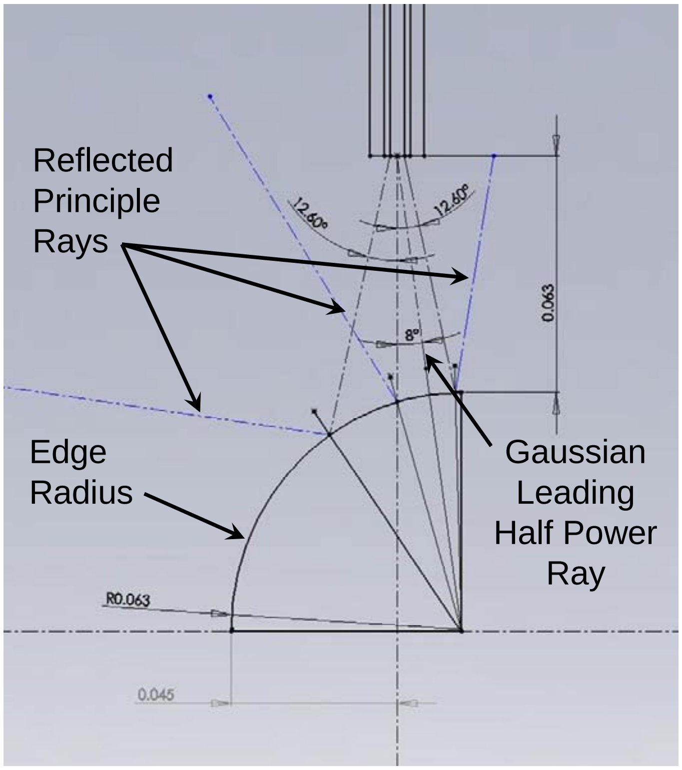

FIG. 9; RAY TRACING OF GAUSSIAN HALF POWER POINT RAY REFLECTING BACK TO PROBE CENTER

This ray tracing analysis provides the basis for a general expression of late edge detection at low signal power levels and is depicted in Fig 10. A simple trigonometric relationship for late edge detection, as a function of edge radius and gap, can be derived by accepting the assumption that low trigger level occurs when the half power Gaussian ray reflects back to the probe center, Equation 1

1) δ = R- ((R+G) $\times$ tan ϕ)
δ = edge detection error
R = edge radius
G = probe to specimen gap
ϕ = 8°

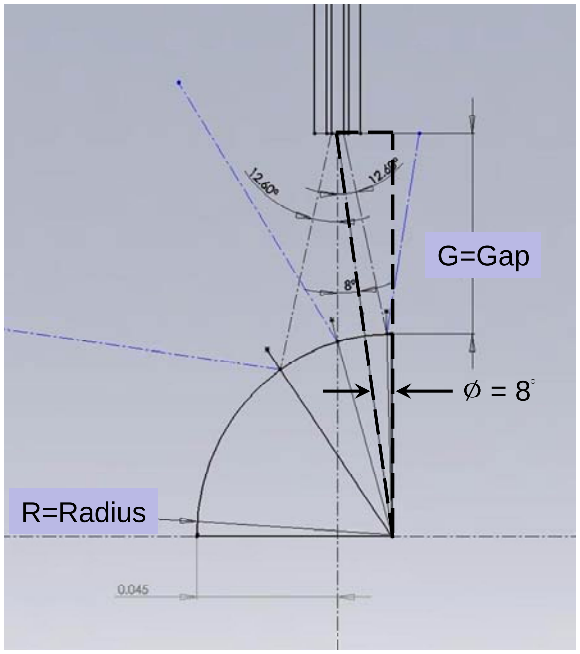

FIG. 10; GEOMETRIC CONSTRUCTION EDGE DETECTION ERROR ASA FUNCTION OF GAP AND RADIUS

This expression should be in agreement with the sharp edge analysis when the radius goes to zero. A conflict between this radius edge and sharp edge analysis is evident since this model predicts the error will be a function of gap when at a sharp edge. Further work will be required to create a consistent set model.

Writing the expression for the probe location relative to the edge radius at the high measured power level starts by seeing that this location is the point when all the receiver fibers are first illuminated by reflected light from the flat surface. This analysis becomes the same as to the sharp edge case for highest power, except the 0.005 inches (0.127mm) is measured past the tangent point of the radius and flat surface. The resulting detection error is the sum of the edge radius plus the constant 0.005 inches (0.127mm), Eq. 2.

2) δ = R + C
δ = edge detection error
R = edge radius
C= sharp edge error constant

The predictions from Eq. 1 and 2 are shown, Fig. 11, as a function of edge radius for 0.0625 inches (1.588 mm) probe specimen gap. Zero on the Y axis of this graph represents the true edge location so negative probe locations occur before the true edge. The predicted early probe location for low trigger levels at zero radius is -0.009inches (0.229mm) instead of -0.005 inches (0.127mm). The slopes of these relationships are the rate of change in edge detection error as a function of radius change. This error rate is unit-less since edge detection location and edge radii are length dimensions. The regressions show an error rate of 1.0 at all the highest trigger levels condition and 0.86 at the lowest trigger levels.

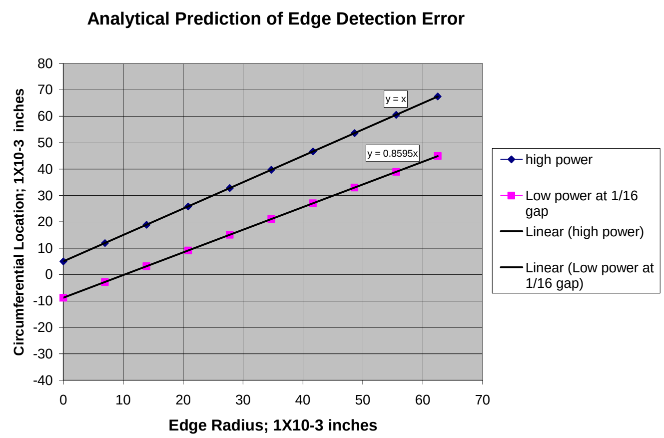

FIG. 11; PREDICTED ERROR AS A FUNCTION OF RADIUS FOR HIGHEST AND LOWEST TRIGGER LEVELS WITH PROBE 0.0625 INCHES FROM SPECIMEN

The prediction can be compared to the test results by re-plotting the laboratory data as a function of edge radii. The data for the 0.0625 inches (1.588 mm) probe gap is shown in Fig. 12. The measured error rate for the high and low trigger levels were determined by performing separate linear regressions. The regressions show an error rate of approximately 0.97 at all the highest trigger level of data set and 0.86 at the lowest trigger level. The error rates are in good agreement with the predictions above.

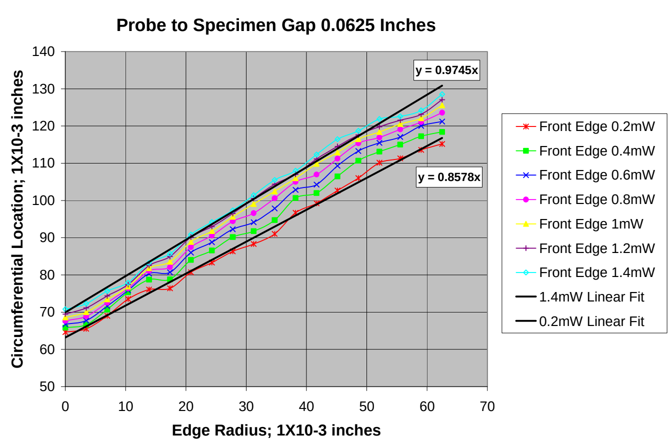

FIG. 12; ERRORS AS A FUNCTION OF CORNER RADIUS AT SPECIFIED OPTICAL POWER LEVELS WITH PROBE 0.0625 INCHES FROM SPECIMEN

The comparison of predicted to laboratory data for the larger probe gaps of 0.1875 and 0.25 inches (4.763 and 6.350 mm) is shown respectively in Figs. 13-16. The predicted high power edge detection error is the same on all plots since this function is independent of probe gap. The high power level data in figs. 14 and 16 are in good agreement predicting error rates of one. The large discrepancy in the intercepts shows that the model assumption caused deficiencies in matching the data. These discrepancies can be ignored since only the slope is needed to quantify the error that propagates into the blade deflection information. The low power level predictions fail at the intercept where radius is zero, but the error rates, slopes, are in reasonable agreement Future work is needed to produce a complex optical model that will resolve these inconsistencies.

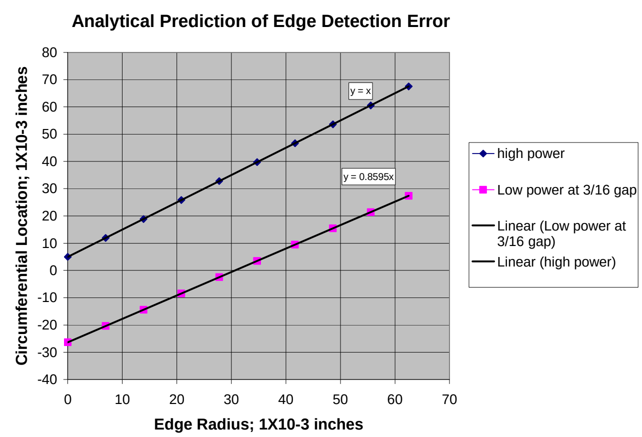

FIG. 13; PREDICTED ERROR AS A FUNCTION OF RADIUS FOR HIGHEST AND LOWEST TRIGGER LEVELS WITH PROBE 0.188 INCHES FROM SPECIMEN

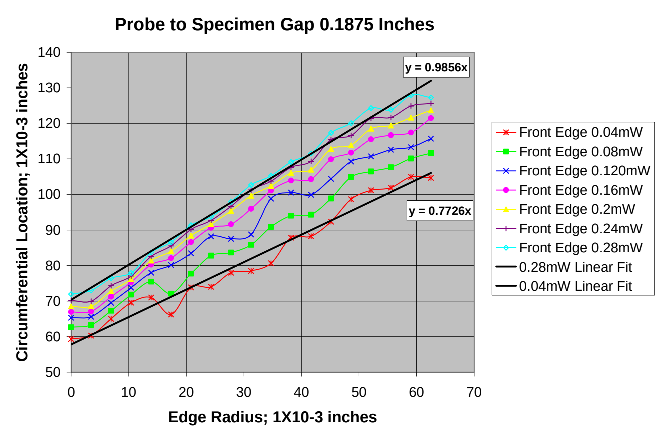

FIG. 14; ERRORS AS A FUNCTION OF CORNER RADIUS AT SPECIFIED OPTICAL POWER LEVELS WITH PROBE 0.1875 INCHES FROM SPECIMEN

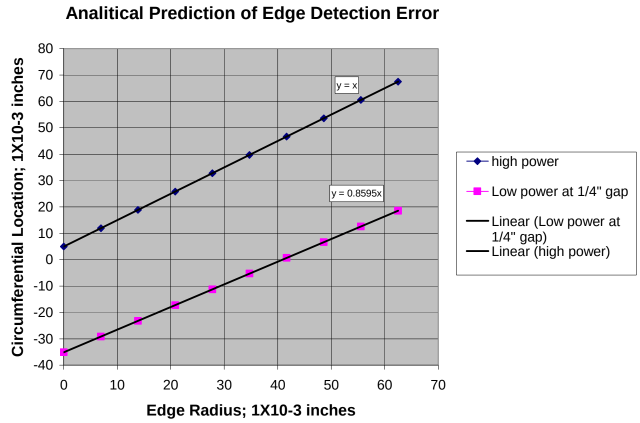

FIG. 15; PREDICTED ERROR AS A FUNCTION OF RADIUS FOR HIGHEST AND LOWEST TRIGGER LEVELS WITH PROBE 0.25 INCHES FROM SPECIMEN

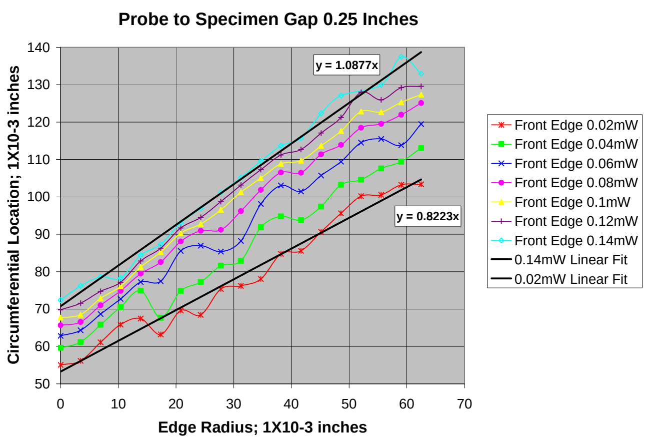

FIG. 16; ERRORS AS A FUNCTION OF CORNER RADIUS AT SPECIFIED OPTICAL POWER LEVELS WITH PROBE 0.25 INCHES FROM SPECIMEN

Error Propagation

Tip timing measurement systems fundamentally measure blade arrival location, hence deflection. The magnitude of measured deflection error caused by changing edge radii is the generate case, in contrast to evaluating stress error propagation that dependent on probe installation, tip timing stress analysis method, airfoil geometry and vibratory mode. This requires limiting the discussion to edge detection errors that propagate into blade deflection-errors, making the assessment independent of the specific application. Limiting the discussion to errors that propagate also allows the constant errors from trigger level to be ignored since all constant errors drop out in the deflection calculation.

Scaling the magnitude of deflection-error as a function of edge-radius change can be done by looking at a hypothetical case in the absence of design data. By assuming a 0.001 inches (0.0254mm) radius change occurring between the vibrating and non-vibrating measurements, the error can be calculated by applying the error rates discussed above. The resulting deflection-errors are between 0.0008 and 0.001 inches (0.0203 and 0.025mm), depending on the trigger level. This small deflection-error can produce significant stress errors for in high frequency vibrations.

Deflection-errors can also be compared to the errors caused by the discreet nature of the digital clock period. A representative blade-tip velocity, such as 16,800 inch/s (426.72m/s), must be assumed to calculate the undetected distance a blade travels between clock steps. Dividing the blade-tip velocity by clock frequency results in the distance a blade-tip travels for a given clock period. This clock error can be thought of as the average equivalent blade-tip deflection-error since the maximum could approach 2 clock steps. Using typical clock speeds of 50, 350, and 500 MHz, the resulting average blade-tip displacement error will be 0.000336, 0.0000483 and 0.0000336 inches/clock-step (0.00853, 0.00123 and 0.00085 mm/clock-step). The average clock-induced deflection-errors are a fraction of the error caused by a 0.001 inch (0.0254mm) radius change. This suggests that improvements from increasing the front-end clock speed have diminishing benefits. Larger improvements will come from reducing errors that originate from probe and blade tip interaction that do not cancel during the deflection calculation.

Conclusions

Errors detecting blade-tip arrival time that vary between vibrating and non-vibrating data will propagate through the measurement system into the stress information. Stress information errors from edge radius will occurs when two conditions are satisfied: (1) the blade-tip edge radius varies in the location that the unfocused optical spot probe intersects the blade and (2) the mode of vibration produces an axial displacement that causes the spot probe's light beam to move along the blade-tip edge(i.e., essentially *all* blade vibrations).

Investing in high-speed front-end data acquisition equipment has reached a point of diminishing returns. The dominant errors that limit tip-timing system accuracy come from errors in arrival location that do not cancel in the vibratory deflections calculation. The greater potential to advance the state of the art is in reducing these errors that do not cancel.

Acknowledgements

The author would like to thank Agilis Measurement Systems, Inc for supplying an unfocused optical spot probe to use in this study.

